Cell size heterogeneity early in development is required for collective cell migration during gastrulation in zebrafish

Triveni Menon[1], Rahul Kumar[1] and Sreelaja Nair[1, *]

[1]Department of Biological Sciences, Tata Institute of Fundamental Research, Homi Bhabha Road, Colaba, Mumbai, 400005, India.

[*]Corresponding author: Sreelaja Nair, email: s.nair@tifr.res.in

Abstract: Metazoan embryos begin life as a single large cell, which divides to generate an entire multicellular organism. This natural progression is characterized by an early, visually striking phenomenon of progressive reduction in cell size, since early cell divisions occur in the absence of cell growth. It is intuitive that early embryogenesis, wherein the phenomenon of growing numbers of progressively smaller cells dominate, cell size may be an important factor for normal development. However, in the absence of experimental efforts directed at altering cell sizes in early embryos, the importance of optimal cell sizes early in development for normal embryogenesis remains an intuitive conjecture at best. We used haploid and tetraploid zebrafish as tools to obtain embryos with smaller or larger than the normal diploid size cells, respectively. Analysis of early development in haploids and tetraploids revealed that when reductive early cell divisions generate a pool of smaller or larger cells in comparison to diploid embryos, embryonic patterning is perturbed due to defective collective migration of cells during gastrulation. During this early phase, the transcriptome of haploid and tetraploid embryos remained largely unperturbed, suggesting that the developmental defects cannot be explained by potential transcriptional changes in response to deviation from a diploid state of the genome. We additionally show that a short exposure to a combination of Aphidicolin and Hydroxyurea during blastoderm stages increases cell sizes in diploid embryos. Such embryos displayed morphological abnormalities that resembled haploid and tetraploid embryos at the end of gastrulation. Conversely, a similar short exposure to a combination of Aphidicolin and Hydroxyurea increased cell sizes in haploid embryos, partially restoring normal patterning. We posit that early reductive divisions set up an optimum range and proportions of cell sizes in early embryos onto which molecular controls are overlaid to execute collective cell migration during gastrulation. Perturbation of the normal cell size landscape triggers aberrant cell migration and gastrulation defects despite normal expression of conserved genes, revealing the importance of optimal cell sizes per se in normal embryonic patterning.

Cell size is a fundamental feature of biological systems, which varies across organisms and across cell types within a multicellular organism (*1, 2*). The size of adult animals is determined genetically but can be heavily influenced by extracellular cues such as nutrient availability and growth factor signaling (*3-9*). Generally, the size of individual cells in adult animals remains comparable, despite dramatic variation in the size of the adult organisms (*4*). This is because organs (and indeed the organism as a whole) can increase in mass by cell growth or by cell proliferation and these two fundamental phenomena can be coupled to or uncoupled from each other in diverse developmental and homeostasis contexts (*10-12*). A phase of development when cell proliferation is always uncoupled from cell growth is the early cell divisions that newly fertilized embryos undergo, which produces increasing numbers of progressively smaller daughter cells. During this rapidly evolving cell size phase, it is unclear the extent to which cell sizes can determine embryonic development. Indeed, it is unclear if cell size optima exist for each phase of early reductive division, which ensures normal transition to the next phase of reductive division, subsequently determining the morphological transformation of a ball of blastoderm cells into a three dimensionally well organized embryo.

We chose to investigate the relevance of cell size optima during the reductive cell division phase on early embryonic patterning using the rapidly dividing zebrafish embryo as our experimental paradigm (*13*). In addition to nutrient and growth factor signaling, genome size is known to determine cell size (*14, 15*). Therefore, to obtain embryos with cell sizes smaller or larger than the normal diploid embryos, we chose to use haploid and tetraploid zebrafish embryos. Our study experimentally proves the existence of cell size regulation during reductive cell division in embryos and show that deviation from an early stage-specific cell size norm can cause defects in embryonic development in zebrafish.

We began our investigations by characterizing cell sizes in diploid zebrafish embryos during early development by immunofluorescence analysis for β-catenin to mark cell boundaries (Fig. 1, Supplementary Fig. 1, 2). We chose the early blastoderm (2 hours post fertilization (hpf) and pre-zygotic genome activation (ZGA) phase), late blastoderm (3, 4 hpf and post-ZGA phase), early gastrula (6 hpf) and early larva (24 hpf) for quantitative analysis of cell size reduction during zebrafish development (Fig. 1, Supplementary Fig. 1, 2). We divided 3, 4 and 6 hpf embryos into four quadrants and imaged a region of interest within each quadrant to sample majority of the blastoderm for quantitative analysis of cell areas (Supplementary Fig. 1D-De, Supplementary Fig. 2A-Ae and 2D-De). Qualitative assessments of the embryos revealed that embryos are composed of comparatively smaller cells as development proceeds (Fig. 1A-F, Supplementary Fig. 1A, 1D-De, Supplementary Fig. 2A-Ae and 2D-De). We quantified the progressive reduction in cell sizes by processing the β-catenin immunofluorescence images using the BioVoxxel toolbox in ImageJ (*16*) to obtain the cell areas at each developmental stage (Fig. 1G-J). To obtain a better understanding of how cell sizes evolve dynamically during normal development, we chose to bin the cells as small, medium and large size cells based on cell areas as follows: at any stage of development, medium category of cells were defined as cells with areas +/- 10% of the average area for that stage of development. Cells with areas less than this bin were categorized as small and cells with areas more than this bin were categorized as large. For example, at 2hpf, the average cell size is 3507.5 μm^2; medium size cell bin = 3156.8 to 3858.3 μm^2, area less than 3156.8 μm^2 = small cells, area greater than 3858.3 μm^2 = large cells. The binning of the cell area values into small, medium and large cells allowed us to set normative area thresholds for each cell size category across the reductive cell division phase in normal diploid embryos (Fig. 1K-O). These area thresholds were integral for subsequent quantitative analysis of cell size deviation from the norm in haploids and tetraploid embryos. Interestingly, at all stages assayed, the relative proportions of each size category remained comparable with small cells making up 35 – 50%, medium cells 12 – 25 % and large cells 35 – 40% of the total cells (Fig. 1P). We next analysed the

extent to which cell sizes shrink at the successive developmental stages assayed. Our analysis of the average areas revealed that between 2 to 6 hpf, cells size decreases linearly by ~3-fold (R^2 of a linear fit from 2 to 6 hpf is 0.99). The ~3-fold reduction in cell areas between 2 to 6 hpf holds true for the individual category of small, medium and large cells as well. Pair-wise analysis of the extent of cell size reduction between successive stages additionally revealed that the 3-fold reduction in cell size is not uniform between successive pairs of stages. Between 3 to 4 hpf, a stage just before epiboly movements mark the onset of collective cell migration that set the stage for gastrulation in zebrafish, cell size reduces by ~1.5 fold.

Haploid and tetraploid zebrafish embryos tend to undergo normal rounds of early reductive divisions and reach blastoderm stages comparable to diploid embryos (*17*). It is known that ploidy affects cell size (*14, 15*). Therefore, unsurprisingly, cell sizes in haploid and tetraploid embryos appeared to be smaller and larger respectively, particularly at 2, 3, 4 and 6 hpf (Supplementary Fig. 1A-C and D-Fe, Supplementary Fig. 2A-Ce and D-Fe). We analysed the cell area in haploid and tetraploid embryos at 2, 3, 4 and 6 hpf by categorizing the cells as small, medium or large in accordance with the area values of their stage matched diploid size categories. In the early haploid blastoderm at 2 hpf, cell sizes of small, medium and large cells were comparable to diploid blastoderm cells of the corresponding sizes (Supplementary Fig. 3A). As development progressed, in the late blastoderm at 3 and 4 hpf and early gastrula at 6 hpf, haploid small and large cells remained significantly smaller than diploid small and large cells, respectively (Fig. 2A-C). Medium cells tended to deviate from the size norm only at 2 and 4 hpf (Fig. 2B and Supplementary Fig. 3A). Thus, during late blastoderm at 3 and 4 hpf and early gastrula at 6 hpf, small and large cells in haploids consistently deviated from the cell size norm (Fig. 2A-C). The reductive cell division phase is followed by a phase during which collective cell migration rearranges cells to morphologically transform the blastoderm into a three dimensionally patterned embryo through gastrulation. In haploids, if the deviation from the cell size norm is to exert an effect on collective cell migration during epiboly and gastrulation, either small or large cells may need

to exist disproportionately in the inherently heterogenous cell size landscape. An analysis of the distribution of cell size categories in haploids revealed that 45 - 83% were small cells, whereas 6 - 40% were large cells between 2 to 6 hpf (Fig. 2G-I, Supplementary Fig. 3E).

In the early tetraploid blastoderm at 2 hpf, there were no small or medium cells and the large cells were significantly bigger than diploid large cells at 2 hpf (Supplementary Fig. 3C). As development progressed, in the late blastoderm at 3 and 4 hpf and early gastrula at 6 hpf, tetraploid large cells remained significantly bigger than diploid large cells at comparable developmental stages (Fig. 2D-F). Small and medium cells were significantly bigger in tetraploids only during 2 and 3 hpf, but were comparable to diploid small and medium cells at 4 hpf and 6 hpf (Fig. 2D-F and Supplementary Fig. 3C). Thus, the size category that deviates most from the norm at all early stages of tetraploid development are large cells. Additionally, large cells are the only category of cells that deviate from the norm during the key stages of 4 hpf when epiboly begins, and 6 hpf when gastrulation begins in the zebrafish embryo. We hypothesized that in order to exert a biologically relevant effect on collective cell migration during epiboly and gastrulation, the large cells of tetraploids may potentially dominate the inherent heterogenous cell size landscape of the embryo. In agreement with this hypothesis, large cells comprise 70 - 98% of the total cells in the tetraploid early blastoderm and gastrula. In haploids and tetraploids, despite these deviations from the cell size norm during 2 to 6 hpf, small and medium cells are comparable to diploids by 24 hpf, while large cells remain larger than their diploid counterparts (Supplementary Fig. 3B, D). Additionally, the proportions of small, medium and large cells in haploids and tetraploids begin to resemble those in diploid embryos at 24 hpf (Supplementary Fig. 3F).

Scaling in hap, tet,

Thus, categorization of cells in haploids and tetraploids according to cell size with respect to those in stage matched diploids show that haploids are composed of predominantly smaller cells and tetraploids of larger cells just before and during gastrulation. Collective behaviours of cells are

influenced by cell sizes in several different contexts, particularly cell migration (*18, 19*). The stages at which we have uncovered cell size abnormalities in haploids and tetraploids progress to gastrulation, where large-scale rearrangements of cells occur to create the primary germ layers of the embryo and the three dimensional embryonic body plan. We monitored embryonic development in live embryos after 4 hpf, a stage during which the cell size distribution in haploids and tetraploids deviated mostly to smaller and larger cells respectively, to understand the effect, if any, on development during gastrulation. Diploid embryos undergo a series of well-characterized collective cell behaviours such as migration over the yolk ball (epiboly) from 4 hpf, followed by involution at the margin and anterior migration, which marks the beginning of gastrulation at 6 hpf, and subsequent dorsal convergence to thicken and elongate the body axis on one side by the end of gastrulation at 10 hpf (Fig. 2M-P). In haploids and tetraploids, the initiation of epiboly, formation of the dorsal shield and anterior migration was delayed (Fig. 2M-P). By the end of gastrulation at 10 hpf, haploid and tetraploid embryos had a comparatively shorter body axis, which was also evident at 24 hpf (Fig. 2M-P and data not shown). Taken together, the live morphologies of haploid and tetraploid embryos suggest defects in collective migration of cells during epiboly and gastrulation.

To confirm this, we performed whole embryo RNA in situ hybridization for a select group of genes to assess for defects in anterior migration and dorsal convergence. At 7 hpf, *gsc* is expressed by the prechordal plate mesoderm cells at the anterior and *foxa2* marks posteriorly juxtaposed axial mesoderm (Fig. 3A). In haploids, the domains of *gsc* and *foxa2* expression remained intermingled and the foxa2 expressing axial mesoderm cells were found in a shorter domain, indicating a failure in anterior migration of prechordal plate cells and axial mesoderm elongation (Fig. 3B). In tetraploids, though there were no overt defects in *gsc* and *foxa2* expression domains, in general *gsc* expression seemed dampened (Fig. 3C). After completion of gastrulation at 10 hpf, the extent of dorsal convergence of cells can be assessed by the distance between the bilateral rows of non-neural ectodermal cells across the dorsal midline, marked by *dlx3b* (Fig. 3D). In both haploids and tetraploids, the non-neural ectoderm cells were located further away from

the midline, indicating a failure to converge dorsally (Fig. 3E, F). Thus, haploid and tetraploid embryos composed predominantly of smaller and larger cells respectively, display a range of cell migration defects during gastrulation.

We further tested the migratory behaviors of haploid and tetraploid cells by generating chimeric diploid embryos in which small groups of differentially labeled diploid-haploid or diploid-tetraploid embryos were co-transplanted. Cells were transplanted into diploid embryos at 4 hpf, just prior to initiation of epiboly movements, and tracked live by time-lapse imaging till end of gastrulation at 10 hpf to check for dorsal convergence, a common phenotype in haploid and tetraploid embryos. Though the initial positions of the diploid-haploid and diploid tetraploid cells were the same, during gastrulation and by the end of gastrulation, haploid and tetraploid cells were consistently found further away from the midline in comparison to the co-transplanted diploid cells (Fig. 3G-L). Taken together, the gene expression analysis and live analysis of cell migratory behaviors provide strong support for our view that haploid and tetraploid cells are impaired in their ability to migrate optimally in a group, perhaps resulting in compromised migration anteriorly and convergence dorsally during gastrulation.

The experimental system we used to uncover the relevance of cell size in driving normal embryogenesis was based on alteration of ploidy in embryos. We chose such an apparently flawed system primarily because, 1) cellular and molecular mechanisms that regulate dynamic cell size scaling during early development is not known in any metazoan, 2) there are no mutants which result in smaller or larger cells during early development to understand the consequence of having smaller or larger than normal cells to embryonic patterning. However, we were concerned that the primary defect in haploids and tetraploids may be errors in dosage compensation due to change in ploidy from a diploid state, which manifests as patterning errors in our analysis. To address this, we performed whole transcriptome analysis in haploids and tetraploids at 3-3.5 hpf, after the zygotic genome becomes active at 2.5 hpf (REF). We chose this stage for transcriptome comparisons also because DNA content affect timing of ZGA (*20*-*22*) and therefore the composition of the transcriptomes in haploids and tetraploids may be different. We also reasoned that the early and late blastoderm stages of 3 to 4 hpf were

the developmental time points prior to gastrulation when the small or large cell size category dominates the haploid and tetraploid cell size landscape and therefore transcriptome composition during this phase would be important to understand. Whole transcriptome comparisons show that the majority of genes are not mis-regulated in response to alteration in ploidy at 3-3.5 hpf in zebrafish haploids and tetraploids (Fig. 3M, N). 21 genes were mis-regulated in haploids and 33 genes were mis-regulated in tetraploids (Supplementary Fig. 4). Amongst the 54 genes that were mis-regulated, only 6 genes were mis-regulated in common between haploids and tetraploids suggesting that the transcriptional response is specific to a haploid or a tetraploid state of the genome and it is not a general response to a non-diploid state (Supplementary Fig. 4). The absence of gross transcriptome alterations also suggests that the basis of the early defects we observe in cell migration and gastrulation is unlikely due to early molecular defects in haploids and tetraploids. A molecular pathway well known to drive collective cell migration in diverse cellular and evolutionary contexts is the Planar Cell Polarity (PCP) pathway (*23*). We next checked whether downstream components of the PCP pathway were differentially expressed in haploids and tetraploids by quantitative real time PCRs. For this analysis, we chose late gastrula stage embryos at 8 hpf, since we had transcriptome information at earlier stages. Additionally, dorsal convergence, which is compromised in both haploids and tetraploids, normally initiates during late gastrula stages (*13*). Transcript levels of 11 genes representing diverse components of the PCP signaling pathway remained unaltered in haploids and tetraploids at 8 hpf (Fig. 3O). Taken together, the transcriptome comparisons and quantitative real time PCR data strongly suggest that transcriptional alterations are unlikely contributors to the cell migration defects and subsequent embryogenesis defects seen in haploids and tetraploids.

To prove that cell size deviations from the norm during the early phases of reductive cell divisions in the blastoderm can trigger collective cell migration defects, which manifests as morphological defects in embryonic patterning, we next attempted to alter cell sizes in diploids to achieve a haploid or tetraploid phenotypic outcome at the end of gastrulation. A

combinatorial treatment of Aphidicolin and Hydroxyurea has been reported to effectively alter cell sizes in the zebrafish notochord (*24*). Our experimental strategy was to briefly expose zebrafish embryos to Aphidicolin and Hydroxyurea at ~3 hpf, a developmental stage we chose based on the cell size analysis. We treated embryos from 3 to 6 hpf (encompasses epiboly and initiation of gastrulation) and from 3 to 10 hpf (encompasses epiboly till completion of gastrulation) and recorded at 10 hpf the live phenotype and extent of dorsal convergence using *dlx3b* as a marker. The previously reported concentrations of 150μM Aphidicolin and 20mM Hydroxyurea (*24*) were found to cause embryonic lethality by 10 hpf (Supplementary Fig. 5A). Standardization experiments were then carried out to arrive at a concentration combination, which would alter cell sizes in the zebrafish blastoderm without inducing drug toxicity (Supplementary Fig. 5A). At all concentrations tested, the combinatorial treatment of Aphidicolin and Hydroxyurea resulted in cell size alteration in zebrafish embryos. However, embryos exposed to a combination of 50μM Aphidicolin and 5mM Hydroxyurea or 25μM Aphidicolin and 2.5mM Hydroxyurea either from 3 to 6 hpf or from 3 to 10 hpf both resulted in negligible toxicity, yet effectively altered cell sizes by 6 hpf, when gastrulation begins (Supplementary Fig. 5).

We chose to alter cell sizes in diploids using 50μM Aphidicolin and 5mM Hydroxyurea with a short treatment from 3 to 6 hpf. After the drug treatment, embryos were allowed to develop in drug-free media till 10 and 11 hpf for live and *dlx3b* expression analysis, respectively. In comparison to DMSO exposure, embryos treated with 50μM Aphidicolin and 5mM Hydroxyurea from 3 to 6 hpf showed a visible increase in cell size at 6 hpf, indicating that the short 3 hour exposure was sufficient to achieve cell size alterations in diploids (Fig. 3P, Q). At 10 hpf, in comparison to DMSO treated diploids, the Aphidicolin and Hydroxyurea treated diploid embryos had shorter body axis, which resembled the phenotypes seen at 10 hpf in haploids and tetraploids (Fig. 3Pa, Qa, compare to Fig. 2O, P). We additionally assessed the extent of dorsal convergence at 12 hpf by assaying for *dlx3b* expression in diploid embryos treated with Aphidicolin and Hydroxyurea from 3 to 6 hpf. DMSO treated embryos resembled untreated control embryos with the non-

neural ectoderm on either side of the midline (Fig. 3R, compare to 3D). However, in diploid embryos treated with Aphidicolin and Hydroxyurea, the *dlx3b* expressing non-neural ectoderm was found further away from the midline, a phenotype that resembled the *dlx3b* expression in haploids and tetraploids (Fig. 3S, compare to 3E, F). It is unlikely that the short (3 to 6 hpf) and lower than reported concentration of Aphidicolin and Hydroxyurea used in our experiments causes transcriptional or other appreciable molecular changes in the embryos. Thus, diploid embryos in which we increased the size of cells during early blastoderm to gastrulation stages by pharmacological interventions failed to execute dorsal convergence optimally. This experiment strongly supports our view that cell size deviations from the norm during early blastoderm to early gastrulation stages can influence collective cell migration during gastrulation.

Since the combinatorial treatment with Aphidicolin and Hydroxyurea always resulted in increase in cell size, we next treated haploid embryos with this combination as well. We reasoned that in haploid embryos the cell size landscape during early blastoderm to early gastrulation stages is predominantly composed of smaller cells. An increase in cell size may contribute to rescue of the cell migration defects and perhaps result in rescue of embryonic patterning as well. In an identical experimental paradigm to diploids in which we treated haploid embryos with 50μM Aphidicolin and 5mM Hydroxyurea from 3 to 6 hpf embryos resulted in cell extrusions by 10 hpf, indicating that haploid embryos were fragile in nature when exposed to drugs (data not shown). We therefore treated haploid embryos with 50μM Aphidicolin and 5mM Hydroxyurea from 3 to 4.5 hpf, an exposure of 1.5 hrs, instead of the 3 hrs which was used for diploids. In haploid embryos, Aphidicolin and Hydroxyurea treatments caused an increase in cell size, which resulted in embryos with partially rescued axis extension at 10 hpf, though the embryos appeared to have other defects such as a smaller head (Fig. 3T-Ua). However analysis of dorsal convergence in Aphidicolin and Hydroxyurea treated haploid embryos clearly showed that the non-neural ectoderm marked by *dlx3b* was closer to the midline than in untreated haploid embryos. This indicates that cell size increase in haploids restored to some extent the ability of cells to converge dorsally, perhaps because the

predominantly small cells in haploids were now balanced with larger cells due to the Aphidicolin and Hydroxyurea treatments.

Co-ordinated migration of cells requires communication between large groups of cells, which may be compromised if a fundamental property such as the absolute size of cells or the relative proportions of cells of a specific size category change in the group. Our study reveals that in zebrafish embryos, iterative rounds of reductive cell divisions generate proportional numbers of small and large cells and a smaller proportion of medium size cells in the blastoderm during epiboly and early gastrulation. When the absolute cell size or proportions of specific cell sizes deviate from the norm early in development (as seen in haploids, tetraploids or Aphidicolin and Hydroxyurea treated diploids), collective migratory properties of cells during gastrulation also deviate from the norm. These result in patterning errors at the end of gastrulation and may contribute to the eventual lethality haploids and tetraploids succumb to. Interestingly, such patterning errors occur in the absence of gene expression changes, indicating that molecular mechanisms that execute the process of gastrulation are unable to overcome the developmental aberration the deviation from the cell size norm causes. We conclude that an optimum heterogenous cell size during early development is required for executing gastrulation movements for normal embryonic development.

Acknowledgements: This work was supported by an India Alliance Wellcome Trust/Department of Biotechnology Intermediate Fellowship IA/I/13/2/501042 awarded to SN and by the Tata Institute of Fundamental Research Mumbai. We wish to thank AM for help with RNA preparations for the transcriptome analysis and SK for the initial help in graphically representing the bioinformatics results. We thank current and past members of SN lab for critical inputs during the course of this study.

Author Contributions:

TM performed all experiments, collected, analysed and compiled the data. SN designed the study, performed experiments, data analysis and compilation

with TM. RK performed the qRT-PCR experiments. SN wrote the manuscript with feedback from TM.

Animal use ethics statement: All animal husbandry, animal handling and experiments in this study were conducted in strict accordance with national and institutional animal use guidelines (approval number TIFR/IAEC/2015-3).

References

1. D. L. Levy, R. Heald, Biological Scaling Problems and Solutions in Amphibians. *Cold Spring Harb Perspect Biol* **8**, a019166 (2015).
2. J. Arendt, Ecological correlates of body size in relation to cell size and cell number: patterns in flies, fish, fruits and foliage. *Biol Rev Camb Philos Soc* **82**, 241-256 (2007).
3. K. Artiles, S. Anastasia, D. McCusker, D. R. Kellogg, The Rts1 regulatory subunit of protein phosphatase 2A is required for control of G1 cyclin transcription and nutrient modulation of cell size. *PLoS Genet* **5**, e1000727 (2009).
4. I. Conlon, M. Raff, Size control in animal development. *Cell* **96**, 235-244 (1999).
5. B. A. Edgar, How flies get their size: genetics meets physiology. *Nat Rev Genet* **7**, 907-916 (2006).
6. P. Jorgensen, J. L. Nishikawa, B. J. Breitkreutz, M. Tyers, Systematic identification of pathways that couple cell growth and division in yeast. *Science* **297**, 395-400 (2002).
7. P. Jorgensen, M. Tyers, How cells coordinate growth and division. *Curr Biol* **14**, R1014-1027 (2004).
8. P. Nurse, The genetic control of cell volume. *The Evolution of genome size*, 185-196 (1985).
9. K. Tumaneng, R. C. Russell, K. L. Guan, Organ size control by Hippo and TOR pathways. *Curr Biol* **22**, R368-379 (2012).
10. J. Dong *et al.*, Elucidation of a universal size-control mechanism in Drosophila and mammals. *Cell* **130**, 1120-1133 (2007).
11. T. T. Su, P. H. O'Farrell, Size control: cell proliferation does not equal growth. *Curr Biol* **8**, R687-689 (1998).
12. Z. Qu, J. N. Weiss, W. R. MacLellan, Coordination of cell growth and cell division: a mathematical modeling study. *J Cell Sci* **117**, 4199-4207 (2004).
13. C. B. Kimmel, W. W. Ballard, S. R. Kimmel, B. Ullmann, T. F. Schilling, Stages of embryonic development of the zebrafish. *Dev Dyn* **203**, 253-310 (1995).
14. T. Cavalier-Smith, Economy, speed and size matter: evolutionary forces driving nuclear genome miniaturization and expansion. *Ann Bot* **95**, 147-175 (2005).
15. S. P. Otto, The evolutionary consequences of polyploidy. *Cell* **131**, 452-462 (2007).

16. J. Brocher, Qualitative and Quantitative Evaluation of Two New Histogram Limiting Binarization Algorithms *IJIP* **8** 30-48 (2014).
17. T. Menon, S. Nair, Transient window of resilience during early development minimizes teratogenic effects of heat in zebrafish embryos. *Dev Dyn* **247**, 992-1004 (2018).
18. A. Leal-Egana *et al.*, The size-speed-force relationship governs migratory cell response to tumorigenic factors. *Mol Biol Cell* **28**, 1612-1621 (2017).
19. O. M. Matsiaka, C. J. Penington, R. E. Baker, M. J. Simpson, Discrete and Continuum Approximations for Collective Cell Migration in a Scratch Assay with Cell Size Dynamics. *Bull Math Biol* **80**, 738-757 (2018).
20. D. A. Kane, C. B. Kimmel, The zebrafish midblastula transition. *Development* **119**, 447-456 (1993).
21. J. Newport, M. Kirschner, A major developmental transition in early Xenopus embryos: II. Control of the onset of transcription. *Cell* **30**, 687-696 (1982).
22. J. Newport, M. Kirschner, A major developmental transition in early Xenopus embryos: I. characterization and timing of cellular changes at the midblastula stage. *Cell* **30**, 675-686 (1982).
23. C. F. Davey, C. B. Moens, Planar cell polarity in moving cells: think globally, act locally. *Development* **144**, 187-200 (2017).
24. Y. Liu, D. S. Sepich, L. Solnica-Krezel, Stat3/Cdc25a-dependent cell proliferation promotes embryonic axis extension during zebrafish gastrulation. *PLoS Genet* **13**, e1006564 (2017).

Materials and Methods:

Zebrafish: Experiments were performed with standard laboratory strains Tubingen and AB of *Danio rerio* raised at 28.5°C

Generation of haploid and tetraploid embryos: All experiments were performed using temporally synchronized embryos obtained by in vitro fertilization as done in (Ref) Haploid embryos were generated by in vitro fertilization of mature oocytes with sperms irradiated with 254nm UV light for 90seconds as done in (*17*). To generate tetraploids, diploid embryos obtained by in vitro fertilization were subjected to a brief heat shock of 18minutes post fertilization at 42°C for 2min (*17*).

Immunostaining and analysis of cell size: Embryos were fixed at 2, 3, 4 and 6 hpf in 4% paraformaldehyde and immunolabelled as was done previously in (Ref). Cell boundaries were labeled with primary antibody rabbit anti-β-catenin (Sigma C2206, 1:1000) and fluorescent secondary antibody donkey anti rabbit Alexa 488 (Invitrogen A21202, 1:100). DNA was labelled using DAPI (Roche, 1:500 of 0.5ug/ml). Semi-flat mounts of embryos were

prepared in 70% glycerol (in1X PBS) containing DABCO (Sigma D27802) anti fade reagent and imaged on Olympus FV1200 confocal microscope. Images were processed and analyzed on Fiji and panels were assembled on Adobe Photoshop CC.

For determining cell surface area and cell perimeter values at different developmental stages, the confocal images obtained were subjected to a Fiji analysis pipeline. The confocal image was opened on Fiji and the total number of stacks were divided into sets of three. The middle stack of the middle set was used for max projection of the image. The image was despeckled and saved as a .tiff file in an empty folder. The folder was used as the 'input' and 'output' destination for the following macro http://imagej.1557.x6.nabble.com/Index-of-hexagonality-SOLVED-td5013442.html. The segmented image obtained was used in the Extended Particle Analyzer plugin in ImageJ and the cells were numberedwhich was then overlaid on the original confocal image to eliminate aberrantly segmented cells. The segmented image was used in the Shape Descriptor Map plugin of the Biovoxxel Toolbox in ImageJ which generated area heat maps and an excel sheet with respective cross-sectional area of each cell.

In situ hybridization: Embryos fixed in 4% paraformaldehyde were processed for whole in situ hybridization as done in (Thisse and Thisse,). Briefly, PFA fixed embryos were dehydrated in 100%meOH overnight and then subjected to a MeOH series followed by incubation in prehybridiztaion and hybridization buffer containing digoxigenin and fluorescein tagged anti sense RNA probes. The tagged RNA was labelled with alkaline phosphatase tagged anti-digoxigenin (Roche 16646820) and anti-fluorescein antibodies (Roche 17110000). Digoxigenin labelled antisense RNA was detected using NBT (Roche 11383213001) and BCIP substrate (Roche 11383221001) color reaction and fluorescein labelled RNA was detected by Sigma Fast staining solution (Sigma F4648). Stained embryos were post fixed in 4% PFA and mounted in 100% glycerol for imaging on Zeiss AxioImager. Images were processed and assembled using Fiji and Adobe Photoshop CC.

Ploidy mosaics and live imaging of gastrulation movements: To generate ploidy mosaics, diploid, haploid and tetraploid embryos were generated as described above. Diploid embryos were injected with 0.5nL of 1%

Tetramethyl-rhodamine-dextran (Invitrogen D1817, diluted in nuclease free water) and haploid/tetraploid embryos were injected with 0.5nL of 1%Fluorescein-dextran (Invitrogen D1820, diluted in nuclease free water) at the one celled stage. At 3.5hpf, labelled diploid and haploid/tetraploid donor embryos were mounted alongside an unlabeled diploid host embryo in 2.5% Methyl cellulose (Sigma M0387) on depression slides. Few cells from both donors were cotransplanted onto the unlabeled host embryo at 4 hpf and imaged on Zeiss Axioimager epifluorescence microscope. Transplanted embryos were incubated at 28.5 °C. Host embryos were screened for fluorescent transplanted diploid and haploid/tetraploid cells at 6 hpf and selected embryos were mounted laterally (shield on right) in 0.5% low melting agarose on depression slides for live imaging. Embryos were imaged on Zeiss LSM880 confocal microscope through gastrulation until the tail bud stage (10 hpf).

Drug treatment: To manipulate cell size in diploid embryos, embryos were generated by in-vitro fertilization and transferred into 0.3% Danieau (17mM NaCl, 0.21mM KCl, 0.12mM $MgSO_4.7H_2O$, 0.18mM $Ca(NO_3)_2.4H_2O$ and 1.5mM HEPES; pH 7.6) medium. At 2.5 hpf, embryos were dechorionated using Pronase (Sigma P6911) and transferred to glass petridishes containing Danieau medium. The Danieau medium was replaced with a mixture of 50µM Aphidicolin (Sigma A0781) and 5mM Hydroxyurea (Sigma H8627) solution prepared in 4% DMSO at 3hpf. The drug solution was washed off at 6 hpf and replaced with Danieau medium. Embryos were mounted in 0.5% low melting agarose on depression slides and imaged live at 3, 6, 10 and 12 hpf and additionally fixed at 12 hpf for whole in situ hybridization.

Transcriptome analysis: Diploid, haploid and tetraploid embryos were generated in 3 independent experiments and total RNA was extracted by Trizol method (Ambion 15596018) at 3hpf. RNA obtained from 3 sets of 30-40 embryos each in every independent experiment was subsequently pooled and its quality and yield was assessed using a Bioanalyzer (Agilent 2100). All sets with RIN value >/= 7 were sent for whole transcriptomic analysis. The strand specific, paired end reads were then analyzed using Galaxy open source platform and the data was assembled and represented using R software.

QRT-PCR: Total RNA was extracted from 30-40 haploid, diploid and tetraploid embryos using Trizol reagent (Ambion 15596018). 1µg of the RNA was used to synthesize cDNA using the SSIII RT First Strand cDNA synthesis kit (Invitrogen 18080051). Following primers were ordered from Invenio Life Technologies and used to perform the qPCR using Kapa Syber (Kappa Biosystems KK4601) reaction mix.

Figure Legends

Figure 1. Analysis of cell cross sectional area in diploids during development.

Confocal images of diploid embryos immunostained with β-catenin antibody (**A-F**). Animal view of whole embryo at 2 hpf used for cell size estimation (**A**) while at other developmental stages, embryos were partitioned into 4 quadrants and each quadrant was imaged at higher magnification (**B-D**, one of four quadrants). Surface cells of the neuroepithelium (beneath the skin) were imaged at 24 hpf (**E**) and one of left/right hemisphere was imaged at higher magnification (**F**). Higher magnification images were segmented and cells numbered (**H**). This segmented mask was overlaid on the original confocal image (**G**) to obtain (**I)**. Aberrantly segmented cells (shown in grey in **H**) were noted and excluded from further analysis. Segmented images was input to the Biovoxxel Toolbox on Fiji/ImageJ and a shape descriptor map (**J)** was generated along with area values. **K-O:** Quantitation of cell cross sectional area in diploid embryos at 2,3,4,6 and 24 hpf. Cell area values from each quadrant obtained from 3 embryos at all developmental stages represented as a histogram (**K-O**, "All"). "Small" "medium" and "large" categories were extracted using mean area of all cells. "Medium" categorized as cells with area +/-10% of mean. Line indicates mean area and error bars denote SEM. **P:** Percentage distribution of each category show equal representation at all developmental stages. **Q-R:** Extent of reduction in cell size during development plotted as 'log fold change in area' vs 'log developmental time'. Filled circle- 2hpf, empty circle 3hpf, empty square-4hpf, empty triangle-6hpf and filled triangle-24hpf.

Figure 2. Haploid embryos are composed of smaller cells while tetraploid embryos comprise larger cells when compared to stage matched diploid embryos.

Cell cross sectional area values obtained by quantitation of haploid and tetraploid embryos were categorized into small, medium and large based on diploid mean for that developmental stage. **A-F:** Cell area values obtained from each quadrant combined from 3 embryos at all developmental stages represented as a histogram with line indicating mean area. Haploid cells in the "small" and "large" categories at 3,4 and 6 hpf are significantly smaller than respective categories of diploid cells (**A-C**, * denotes $p<0.05$, Mann-Whitney test). "Large' tetraploid cells are significantly larger than diploid cells of the same category at 3-6hpf (**D-F**, * denotes $p<0.05$, Mann-Whitney test). **G-I:** Percentage distribution of number of cells in each category showing haploids contain more "small" cells while "large" cells predominate in tetraploid embryos. **J-L:** Reduction in cell area of haploid and tetraploid embryos compared to diploids across developmental stages represented as 'log fold change cell area' v/s 'log developmental time'. "Small" and "large" cells in tetraploid show decreased extent of cell size reduction (R^2=0.99 and slope=). **M-P:** Haploid and tetraploid cells look morphologically indistinguishable from diploids till 3 hpf (**M**) but initiate epiboly later than controls (**N**) and continue to progress slower than controls after gastrulation begins (**O,P**).

Figure 3. Haploid and tetraploid embryos are defective in collective migration during gastrulation

Analysis of gene expression domains (**A-F**) by anti-sense RNA in situ hybridization shows *foxa2* (purple), *gsc* (red), *dlx3b* (purple) and *myoD* (red) expression in diploid, haploid and tetraploid embryos. Anterior migration of the prechordal plate cells (red, *gsc* positive) in haploids (**B**, 62/63, N=2) and tetraploids (**C**, 37/59, N=2) and of the axial mesodermal cells (purple, *foxa2* positive) in haploids (**B,** 62/63) was delayed at 8 hpf when compared to diploids (**A,** 34/34). Expression domain of *dlx3b* (purple, non-neural ectodermal cells) in haploids (**E**, 53/67, N=4) and tetraploids (**F**, 32/38, N=3) was broader than diploids (**D**, 56/56, N=4). **G-L:** Rhodamine-dextran (1%) labelled diploid cells (red) were cotransplanted with fluorescein-dextran (1%) labelled haploid (**G,** green) and tetraploid (**J,** green) cells into diploid hosts at 4hpf and imaged live on confocal microscope as lateral mounts (shield on right) till end of gastrulation (**I, L**). Shown are snapshots from the timelapse movie at 6 hpf and 10 hpf (**H, I, K, L**). Haploid (green in **H, I**) and tetraploid

(green in **K, L**) cells appear farther away from the midline than diploid cells (red in **H, I** and **K, L**). Whole genome RNA-sequencing in diploid, haploid an tetraploid embryos at 3 hpf did not reveal significant perturbation of gene expression levels (black dots in volcano plot **M,N**) except for a few genes (red in **M, N**). **O:** Quantitative RT-PCR at 8 hpf for genes involved in gastrulation movements in haploid (filled black circles) and tetraploids (empty circles) reveals no significant difference in gene expression levels. **P-W:** 4% DMSO (**P, Pa, R, T, Ta and V**) or 50µM Aphidicolin+5mM Hydroxyurea (**Q, Qa, S, U, Ua and W**) treated live diploid (**P-S**) and haploid (**T-W**) embryos. Drug treatment increases cell size in both diploid and haploid embryos (**P, Q, T and U**). Drug treatment in diploids causes axis elongation defects (**Qa**) whereas in haploids it partially rescues the same (**Ua**). *dlx3b* expression domain is farther apart in drug treated diploid embryos (**S**, 21/45, N=3) when compared to DMSO treated diploid embryos (**R**, 29/29, N=3). Drug treatment in haploids partially rescues *dlx3b* expression domain (**W**, 21/27) when compared to DMSO treated haploid embryos (**V**, 16/26).

Figure 4. Cell size landscape established during early embryogenesis is required for collective cell migration during gastrulation.

Schematic representation of haploid (**A**), diploid (**B**) and tetraploid (**C**) embryos at 4hpf with haploids being primarily composed of small cells (**A**; inset), diploids having cells of all categories (**B**; inset) and tetraploids being primarily composed of large cells (**C**; inset). Orange-small cells, blue-medium and purple- large cells. Haploids containing more number of “small” cells (**D**) are delayed during progression of epiboly and fail to migrate collectively resulting in a shortened body axis. Haploids treated with Aphidicolin + Hydroxyurea, now comprise of more “large” cells (**E**) compared to untreated haploids and mimic diploids which partially rescues collective cell migration. Diploids containing a mix of all size categories (**F**) undergo normal collective migration during gastrulation and forms an embryo with a well-defined axis. However diploids when treated with Aphidicolin + Hydroxyurea mimic tetraploids (inset) and comprise of more “large” cells (**G**) resulting in defective cell migration and henceforth undergo defective axis elongation. Tetraploids contain more number of “large” cells (**H**) which causes delayed progression of epiboly and defective collective migration causing axis elongation defects.

SupFigure01: Qualitative assessment of cell cross sectional area in diploid, haploid and tetraploid embryos reveals that haploid embryos have smaller cells and tetraploid embryos have larger cells than diploids at 2 and 3hpf.

A-C: Cell cross sectional area estimation at 2 hpf was done from animal view confocal images of diploid, haploid and tetraploid embryos immunostained with β-catenin. At 3hpf, β-catenin stained whole embryos (**D-F**) were partitioned into 4 quadrants- TL-Top left, TR-Top right, BL-Bottom left and BR-Bottom right (**Da, Ea, Fa**). Each quadrant was imaged at higher magnification (**Db-De**, **Eb-Ee** and **Fb-Fe**) and the confocal images qualitatively revealed that haploid cells are smaller and tetraploid cells are larger than diploids.

SupFigure02: Qualitative assessment of cell cross sectional area in diploid, haploid and tetraploid embryos reveals that haploid embryos have smaller cells and tetraploid embryos have larger cells than diploids at 4 and 6hpf.

At 4hpf and 6hpf, β-catenin stained whole embryos (**A-F**) were partitioned into 4 quadrants- TL-Top left, TR-Top right, BL-Bottom left and BR-Bottom right (**Aa, Ba, Ca, Da, Ea and Fa**). Each quadrant was imaged at higher magnification (**Ab-Ae, Bb-Be, Cb-Ce, Db-De, Eb-Ee** and **Fb-Fe**).

SupFigure03: Cell cross sectional area in haploid embryos do not vary before zygotic genome activation and homeostasize by 24 hpf.

Small, medium and large categorization of cells in haploid and tetraploid embryos based on diploid mean at 2hpf and 24hpf. Histograms denote range of cell area with the line indicating mean area for haploids (**A, B**) and tetraploids (**C, D**). Tetraploid “large” cells are significantly larger than diploid cells (**D-F**, ***** denotes $p<0.05$, Mann-Whitney test) at 2 hpf and 24hpf. **E, F:** Percentage distribution of number of cells in each category at 2hpf (**E**) and 24hpf (**F**).

SupFigure04: Few genes are mis-regulated in haploid and tetraploid embryos suggesting that dosage compensation mechanisms are active during early embryogenesis.

Heat map showing differences in FPKM values of genes obtained by whole transcriptomic analysis (N=3) in diploid, haploid and tetraploid embryos at 3 hpf. Genes are arranged based on their expression level in diploids such that

expression level decreases from top to bottom. A total of 54 genes were mis-expressed; 21 genes in haploids and 33 genes in diploids of which 6 genes were commonly mis-regulated.

SupFigure05: Aphidicolin + Hydroxyurea treatment causes increase in cell size and recapitulates axis elongation defects in diploids at all doses.

A: Schematic representation of Aphidicolin + Hydroxyurea treatment at different concentrations starting from 3hpf to 10hpf. **B:** Schematic representation of Aphidicolin + Hydroxurea treatment from 3 to 6hpf using 50μM Aphidicolin+5mM Hydroxyurea and 25 μM Aphidicolin+ 2.5mM Hydroxyurea. **C-H:** Diploid embryos treated with 4% DMSO for 3-6hpf (**C-E**) and 3 to 10hpf (**F-H**). **I-N:** Diploid embryos treated with 25 μM Aphidicolin+ 2.5mM Hydroxyurea from 3 to 6hpf (**I-K**) and 3 to 10hpf (**L-N**). **O-T:** Diploid embryos treated with 4% DMSO (**O-Q**) and 50μM Aphidicolin+5mM Hydroxyurea (**R-T**) from 3- 10hpf have axis elongation defects.

Figure 1

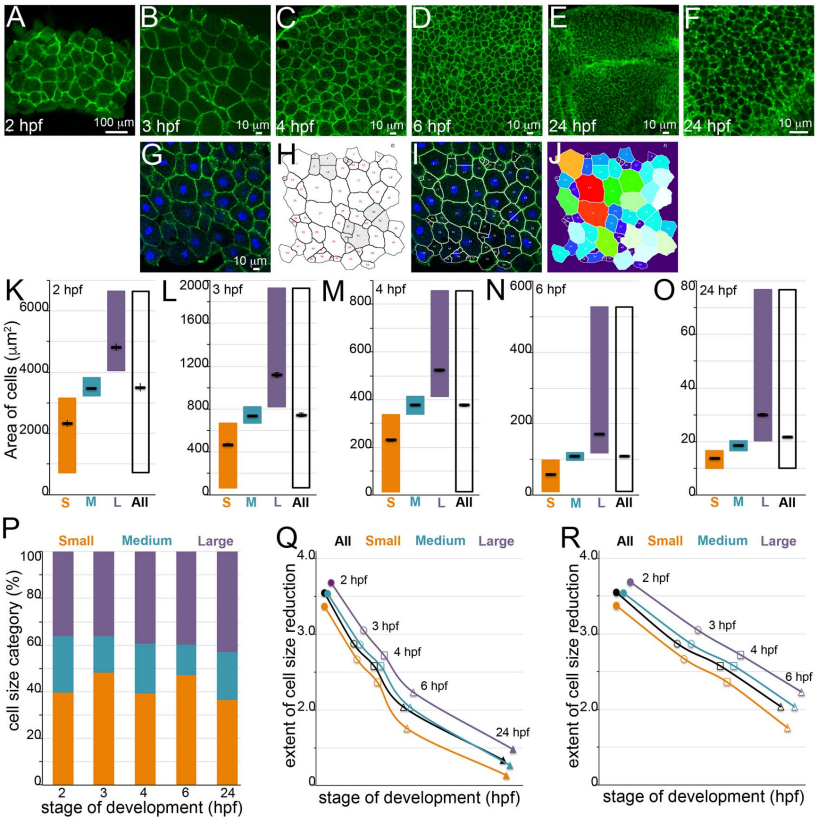

Figure 2

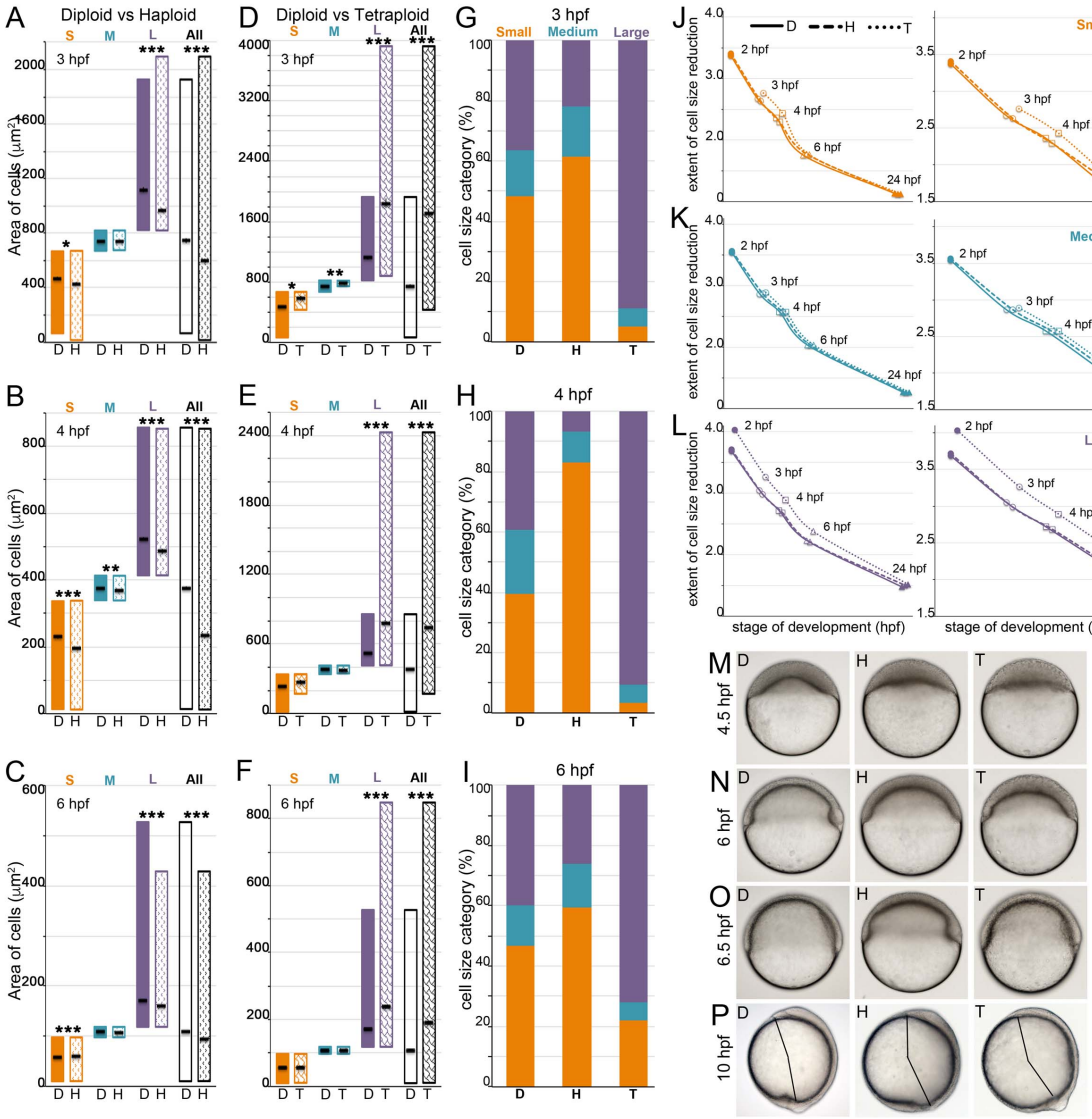

Figure 3

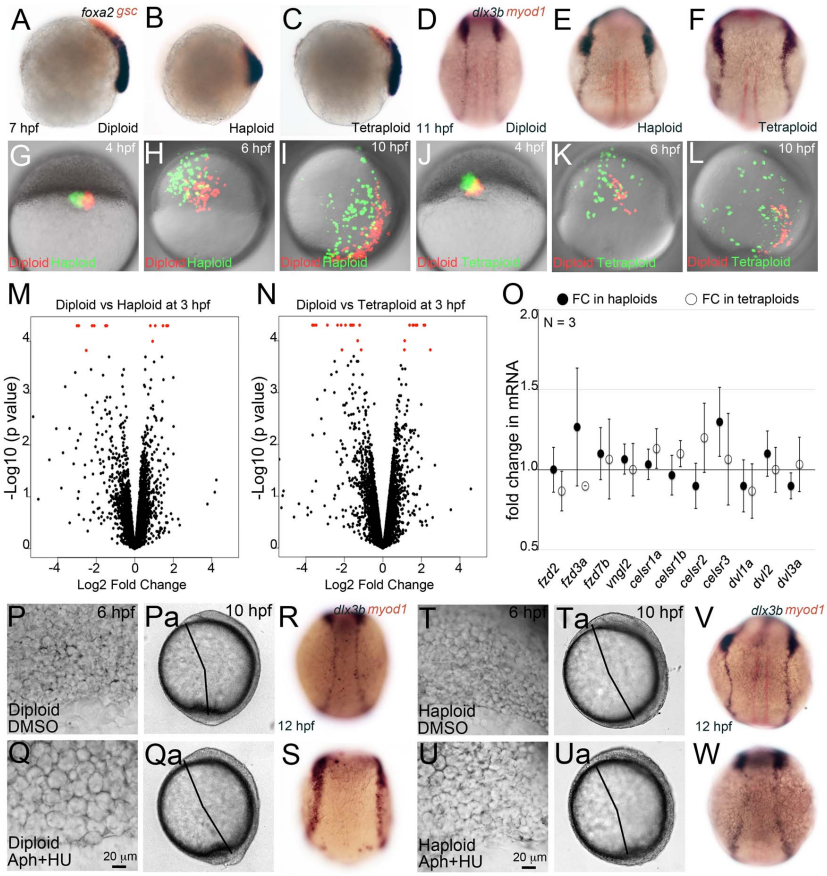

Figure 4

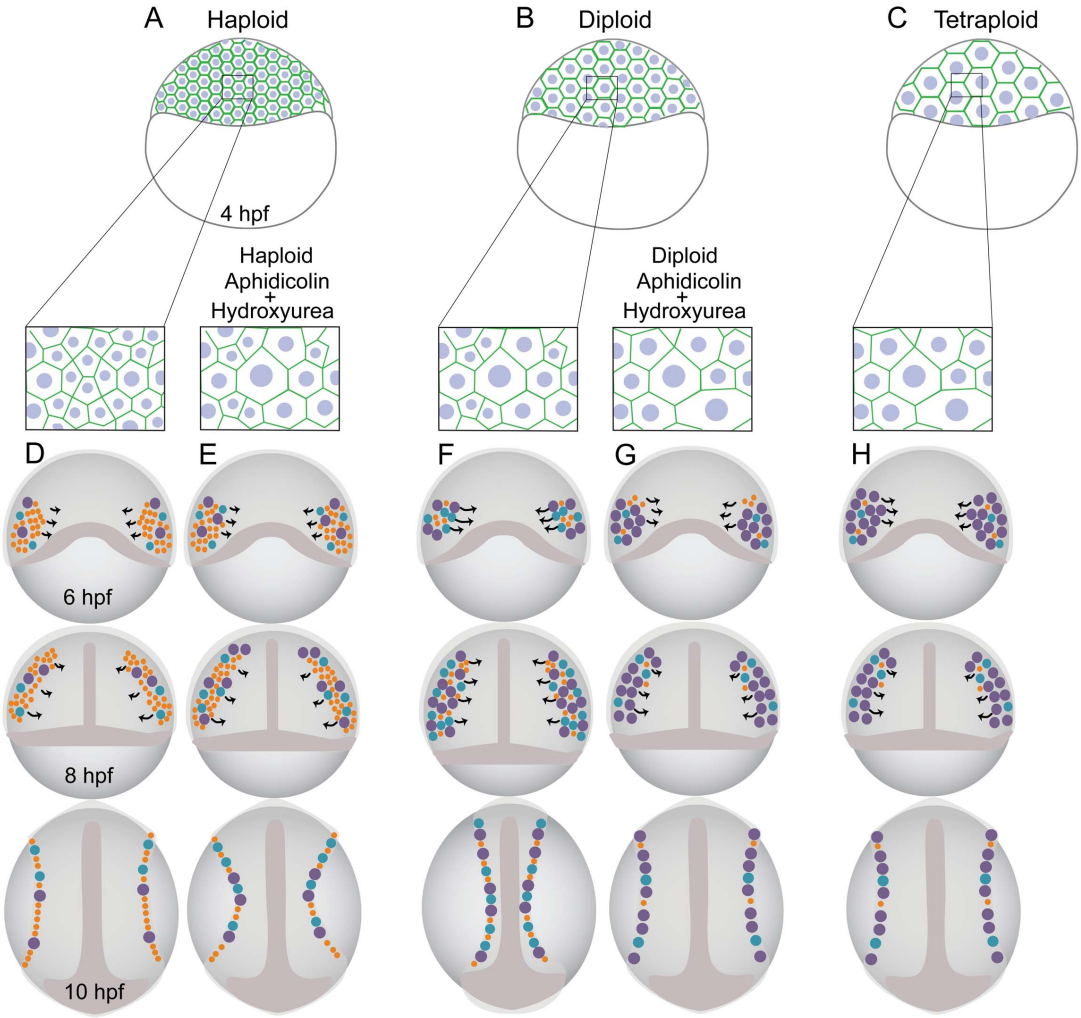

Supplementary Figure 1

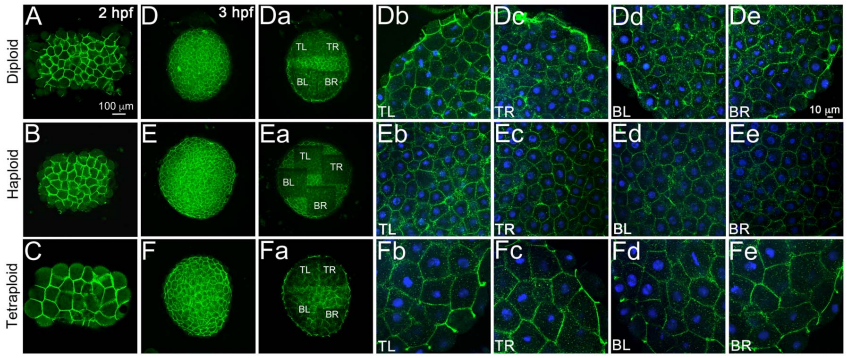

Supplementary Figure 2

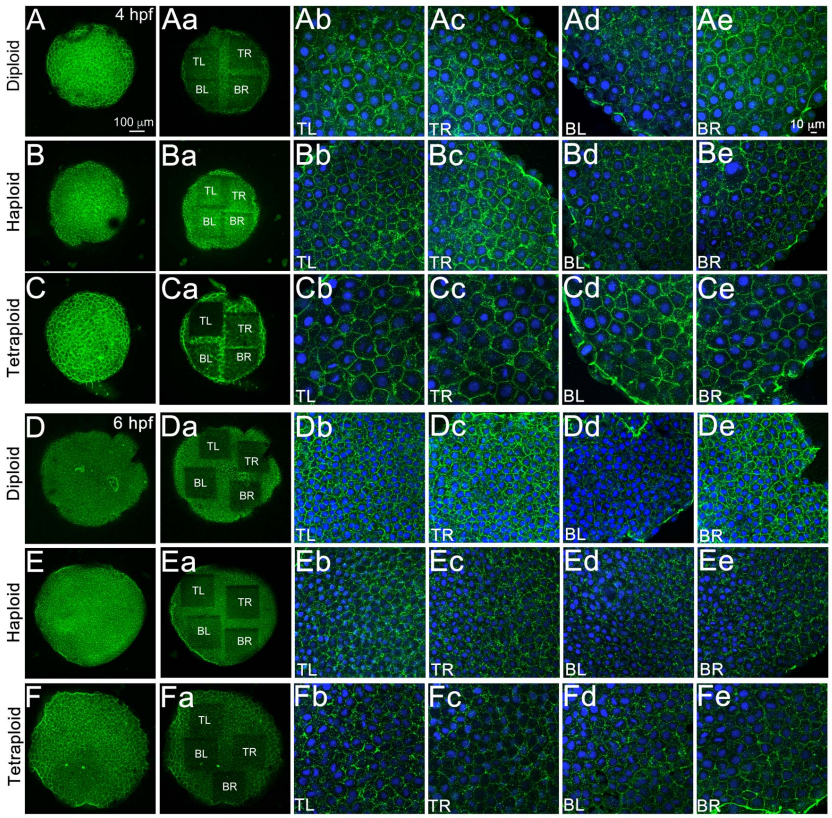

Supplementary Figure 3

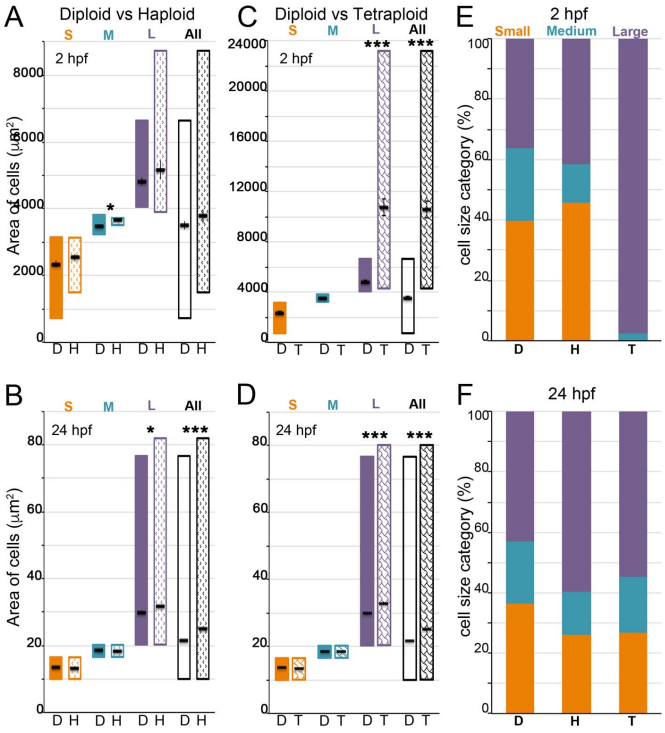

Supplementary Figure 4

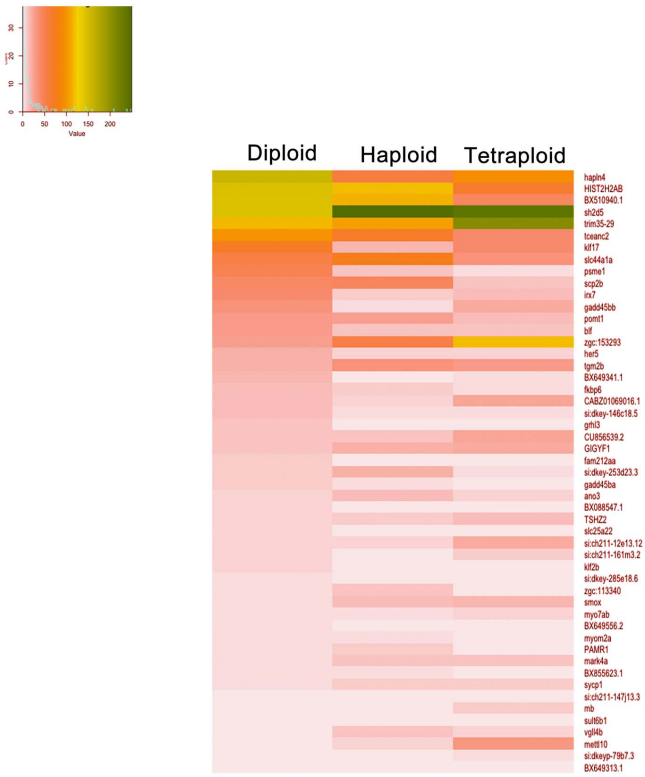

Supplementary Figure 5